2024 10th International Conference on Control, Decision and Information Technologies (CoDIT) | 979-8-3503-7397-4/24/$31.00 ©2024 IEEE | DOI: 10.1109/CoDIT62066.2024.10708604

A Cost-Effective Automatic Calibration Platform for Inertial Measurement Units

Salvatore R. Bassolillo
Department of Science and Technology
University of Naples "Parthenope"
Napoli, Italy
salvatorerosario.bassolillo@collaboratore.uniparthenope.it

Egidio D'Amato
Department of Science and Technology
University of Naples "Parthenope"
Napoli, Italy
egidio.damato@uniparthenope.it

Immacolata Notaro
Department of Engineering
University of Campania "L.Vanvitelli"
Aversa (CE), Italy
immacolata.notaro@unicampania,it

***Abstract*—In the last decades, the growing use of small Unmanned Aerial Vehicles (UAVs) has resulted in an escalating demand for low-cost Inertial Measurement Units (IMUs), usually made of Micro Electro-Mechanical Systems (MEMS) to measure accelerations, angular velocities and, optionally, magnetic field components along three axes. An accurate calibration of these devices is needed for the precise determination of aircraft attitude. Although their versatile applications, MEMS-based IMUs exhibit a high level of noise, including both systematic and stochastic errors. Systematic errors need an appropriate calibration process to be identified and eliminated. This paper presents a portable low-cost IMU calibration platform to provide the parameters to mitigate the errors that characterize this kind of devices. Using three servomotors positioned to enable rotations around three orthogonal axes, the system allows for calibrating IMUs both statically and dynamically. To prove the effectiveness of the proposed platform, a performance evaluation is provided, showcasing the difference in estimating the attitude of an IMU, calibrated with and without the use of the platform.**

***Index Terms*—Inertial Measurement Unit (IMU), Calibration.**

I. Introduction

In recent years, Unmanned Aerial Vehicles (UAVs) have experienced increasing success due to their versatility of use in both military and civil fields. To effectively control UAVs in free space, it is essential to have accurate attitude information, computed by integrating raw data coming from Inertial Measurement Units (IMUs) [1]. IMUs are usually composed of a three-axis accelerometer in combination with a three-axis gyroscope, providing measurements of specific force and rotational speed [2]. Sometimes, magnetometers are present to measure the magnetic field and provide information about heading.

The raw data coming from low-cost Micro Electro-Mechanical Systems (MEMS) IMUs are usually affected by several errors: large bias, the non-orthogonality of the axes, misalignment and noise [3]. Indeed, when using MEMS IMU, a fundamental process is related to the characterization and removal [4] of the measurement errors. Without a proper calibration procedure, the sensed data coming from IMUs cannot produce effective attitude information [5].

The main types of errors in an IMU can be classified as stochastic noises and systematic errors, independent of each other. While stochastic are non-deterministic, systematic errors can be determined and eliminated using a proper calibration procedure. Calibration techniques, properly defined in IEEE-standard [6] for inertial measurement systems, are developed by considering accuracy class, available test and measurement equipment, existing data analysis algorithms, and specific standards [7].

The precise calibration of IMU sensors is essential for obtaining accurate and reliable measurements, particularly in hostile environments [8]. Furthermore, effective calibration is required also to implement robust fault detection systems to prevent and mitigate the effects of faults [9, 10, 11, 12].

Calibration procedures for high-end navigational [13] and tactical grade IMUs [14] are expensive and time-consuming processes since manufacturers use dedicated hardware and perform in-house calibration procedures for individual sensors. In order to provide precise references, the authors in [15] presented an IMU calibration procedure using an expensive multi-axes motion stage, while in [16] the authors proposed a camera-based robot arm to complete the calibration procedure.

On the other hand, to efficiently use consumer-grade IMUs [17], it is necessary to keep low both costs and time, developing fast and cost-effective procedures that can be applied even in an in-house context. In this regard, over the years, many researchers attempted to calibrate low-cost IMUs with the least possible equipment. A calibration algorithm without the use of external equipment was proposed in [18], formulating parameter estimation as a cost function minimization problem, solved using Newton's method. In [19], the authors

This work was supported by the research project - ID:20222N4C8E "Resilient and Secure Networked Multivehicle Systems in Adversary Environments" granted by the Italian Ministry of University and Research (MUR) within the PRIN 2022 program, funded by the European Union through the PNRR program.

proposed a low-cost method that uses a 3D-printed cube as a calibration tool; the work also integrates Simultaneous Localization and Mapping (SLAM) technology to generate the IMU rotation reference angle. A three-axis rotating platform was presented in [20] for the calibration of IMUs based on MEMS accelerometer, gyroscope, and a compass; the platform uses servomotors for rotation in the three axes and provides orientation feedback through incremental encoders. The authors in [21] presented a low-cost and portable IMU calibration icosahedron platform and, to take into account calibration errors due to environmental unknown perturbation, they used an iterative Levenberg–Marquardt algorithm for the online calibration of low-cost IMUs.

In this study, we introduce a low-cost platform designed to estimate the calibration parameters of an Inertial Measurement Unit (IMU), with the scope of being readily reproducible and cost-effective. The proposed system is built considering a system akin to a three-axis gyroscope, featuring a servo-actuator and an encoder for each axis. It can be used to simultaneously collect data from the IMU under test.

The paper is organized as follows: Section 2 summarizes the sensor error models, along with their respective calibration procedures. Section 3 provides an overview of the calibration platform design. In Section 4, the results of the calibration are presented, including an attitude estimation comparison with an uncalibrated IMU. Finally, Section 5 outlines some conclusions.

II. Sensor Error Model & Procedure for Parameters Estimation

Despite the significant advantages of MEMS IMUs in terms of small size and affordable costs, their performance is degraded by errors that must be characterized before their use. Indeed, all types of accelerometers and gyroscopes provide raw data affected by different kinds of errors, such as biases, scale factor, and cross-coupling errors [22], consisting of four different contributions: fixed component, temperature-dependent variation, a run-to-run variation, and an in-run variation. While the in-run variation requires other navigation sources for compensation, the first three sources of error can be compensated through laboratory calibration procedures before using the IMU. In addition to the classic instrumentation errors that affect accelerometers and gyroscopes, such as scale factor, cross-coupling, and bias, magnetometers are subject to a magnetic deviation produced by onboard hardware in the hosting platform [23]. This magnetic deviation is composed of a permanent contribution and an induced one, named, respectively, hard iron and soft iron. The first contribution, resulting from permanent magnets and magnetic hysteresis, is equivalent to a bias, while the second one considers the influence that the surrounding ferromagnetic compounds have on the sensed magnetic field by the sensor.

Denote with $\tilde{\boldsymbol{y}}^a$, $\tilde{\boldsymbol{y}}^g$ and $\tilde{\boldsymbol{y}}^m$ the calibrated measurements from accelerometer, gyroscope and magnetometer, respectively. Taking into account the main error sources, the output of the generic sensor δ can be modeled as follows:

$$\tilde{\boldsymbol{y}}^\delta = \boldsymbol{K}^\delta \overline{\boldsymbol{y}}^\delta + \boldsymbol{b}^\delta + \boldsymbol{\nu}^\delta \tag{1}$$

where $\delta \in \{a, g, m\}$ $\overline{\boldsymbol{y}}^\delta$ represents the non-calibrated measurements from sensor δ, $\boldsymbol{K}^\delta$ is the scaling matrix, $\boldsymbol{b}^\delta$ represents the bias and $\boldsymbol{\nu}^\delta$ is the measurement noise.

The calibration process aims to eliminate systematic errors, allowing for a precise estimation of fundamental parameters, such as the bias vector $\boldsymbol{b}^\delta$ and the scaling matrix $\boldsymbol{K}^\delta$. The noise $\boldsymbol{\nu}^\delta$ represents unpredictable and inherent randomness associated with the measurement process. Unlike systematic errors, which cause consistent deviations from true values in the same direction, the measurement noise introduces a lower variability that is not predictable, but it can be modeled with a probability distribution. Consequently, the noise is neglected during the calibration process.

The estimation of the scaling matrix and the bias vector associated with the gyroscope and the accelerometer can be modeled as two linear regression problems. Consider N raw measurements $\overline{\boldsymbol{y}}^\delta(j)$, with $j \in \{1, ..., N\}$, provided by sensors δ, with $\delta \in \{a, g\}$. Each $\overline{\boldsymbol{y}}^\delta(j)$ is acquired in a known configuration $\tilde{\boldsymbol{y}}^\delta(j)$, defined by data collected from the calibrating platform.

The linear regression problem can be defined as follows:

$$\boldsymbol{B}^\delta = \boldsymbol{A}^\delta \boldsymbol{\eta}^\delta \tag{2}$$

where

- the vector of parameters $\boldsymbol{\eta}^\delta = [\boldsymbol{k}_1^{\delta^T}, \boldsymbol{k}_2^{\delta^T}, \boldsymbol{k}_3^{\delta^T}, \boldsymbol{b}^{\delta^T}]^T$, where $\boldsymbol{k}_i^\delta = [k_{i1}^\delta, k_{i2}^\delta ... k_{i3}^\delta]$ is the i-th row of scaling matrix $\boldsymbol{K}^\delta$;
- $\boldsymbol{B}^\delta = [\tilde{\boldsymbol{y}}(1)^T, ..., \tilde{\boldsymbol{y}}(N)^T]^T$;
- $\boldsymbol{A}^\delta = \left[\left(\boldsymbol{A}^\delta(1)\right)^T, ..., \left(\boldsymbol{A}^\delta(N)\right)^T\right]^T$ is a matrix containing the non calibrated sensor outputs, with

$$\boldsymbol{A}^\delta(1) = \begin{bmatrix} \overline{\boldsymbol{y}}^\delta(1) & \boldsymbol{0}_{1\times3} & \boldsymbol{0}_{1\times3} & 1 & 0 & 0 \\ \boldsymbol{0}_{1\times3} & \overline{\boldsymbol{y}}^\delta(1) & \boldsymbol{0}_{1\times3} & 0 & 1 & 0 \\ \boldsymbol{0}_{1\times3} & \boldsymbol{0}_{1\times3} & \overline{\boldsymbol{y}}^\delta(1) & 0 & 0 & 1 \end{bmatrix}$$

With regard to the magnetometer calibration procedure, the identification of the parameters can be formulated as a nonlinear optimization problem.

In a free-perturbation environment, the magnitude of the magnetometer measurement vector $\|\tilde{\boldsymbol{y}}^m\|$ must be equal to the magnitude of the Earth's magnetic field μ. Let us consider N_m as the number of acquired measurements and $\tilde{\mu} = \|\mathcal{M}_E\|$ as the magnitude of the Earth's magnetic field, the cost function to be minimized is defined in Eq. (3).

$$J = \sum_{j=1}^{N_m} (\tilde{\mu} - ||\boldsymbol{y}^m(j)||) \tag{3}$$

III. Calibration Platform Design

Traditional calibration methods need high-precision equipment to perform orientation and rate movements necessary to the calibration model in order to estimate the parameters [24, 25]. In this section, the design and realization of the platform dedicated to calibrating inertial sensors is illustrated.

During the design, the following requirements were considered:

- R1. Actuation Precision: the platform must employ servo-actuators with high precision, ensuring accurate manipulation and measurement of platform angles.
- R2. Platform simpleness: the design should prioritize simplicity and ease of replication, using readily available components to enhance cost-effectiveness and accessibility.
- R3. Multiaxial movement: the platform should facilitate movement around three orthogonal axes to cover the full range of orientation adjustments required for sensor calibration.
- R4. Servo-actuator model: servo-actuators with compact design, lightweight nature, and suitability for small-scale applications should be considered.
- R5. Sequential actuation: actuators should be arranged in a sequential manner, with each actuator influencing the movement of the subsequent one to achieve the desired multi-axial motion.
- R6. Angle resolution: each servo-actuator must be equipped with an encoder featuring a resolution at least of 0.1 deg.
- R7. Customizable position control: the platform control system should allow for full customization of position control, enabling the command of actuators in terms of angular acceleration, velocity or position as needed.
- R8. Mechanical rigidity: the mechanical structure of the platform must exhibit high rigidity to ensure stable and repeatable sensor calibration procedures.
- R9. Mounting structure for IMU: A designated mounting structure must be integrated to correspond to the body reference system on which the Inertial Measurement Unit (IMU) for calibration is installed.

These requirements should ensure the effectiveness, precision, and reliability of the sensor calibration platform.

Table I summarizes the key features and design considerations incorporated into the calibration platform, demonstrating how each requirement has been addressed.

TABLE I: Features and Compliance Specifications

Requirement	Compliance
R1, R4	Dynamixel servo-actuators (XL330-M288-T model) are employed, equipped with an encoder featuring 4096 steps per revolution, providing a resolution below 0.1 deg.
R1, R6, R7	The onboard controller of the servo-actuators can be customized to achieve the desired performance in terms of position, velocity, and acceleration.
R2	Emphasis on simplicity and ease of replication was considered in the design.
R2, R8	Cost-effective plastic-based additive manufacturing was used. Polylactic Acid (PLA) has been chosen for its stiffness properties, and the structure has been designed with appropriate thicknesses to minimize flexibility and displacement during manipulation.
R3, R5	Platform enables movement around three orthogonal axes for comprehensive orientation adjustments. Actuators are arranged sequentially, influencing each other for multi-axial motion.
R7	Firmware developed for the Nucleo G431KB board allows full customization of position control, supporting angular acceleration, velocity, or position commands.
R9	A square plate, measuring 10x10 cm, corresponding to the body reference system, connected to the actuator responsible for the movement around the x-axis, has been manufactured with various connection holes to simplify the quick attachment and detachment of the IMU for calibration.

To define the orientation of the IMU, two reference frames are considered:

- North-East-Down (NED) Reference Frame, located on the surface of the platform base, with X_E and Y_E axes parallel to the surface and Z_E-axis pointing downward.
- Body Reference Frame, centered in the center of the square plate connected to the third servo-actuator, with X_B and Y_B axes parallel and Z_B axis orthogonal to its surface, to form a right-handed reference frame.

The transformation from NED to body frame can be obtained as a sequence of three ordered rotations, called $3-2-1$ [26], described by the so-called Euler angles ψ, θ and ϕ.

- a rotation around the Z_E axis by the yaw angle ψ, from $OX_EY_EZ_E$ to $OX'Y'Z'$;
- a rotation around the Y' axis by the pitch angle θ from $OX'Y'Z'$ to $OX''Y''Z''$;
- a rotation around the X'' axis by the roll angle ϕ from $OX''Y''Z''$ to $OX_BY_BZ_B$.

As shown in Figure 1, from a mechanical perspective, the platform features a circular base of diameter 250 mm, concealing the first servo-actuator responsible for the rotation around the Z_E-axis. This actuator is rigidly connected to a rectangle-shaped ring with rounded corners, mounted perpendicularly to the base, which supports the second servo-actuator for movement around the Y'-axis. A second ring, linked to this actuator, supports the final servo-actuator for the movements around the X''-axis. Lastly, a square plate connected to the last actuator corresponds to the body reference system on which the Inertial Measurement Unit (IMU) for calibration is to be installed. Figure 2 illustrates the 3D printed platform after being built.

Servo-actuators are connected to a Nucleo G431KB board by STMicroelectronics, through a half-duplex serial port. In terms of software, a firmware has been developed to communicate with the servo-actuators, controlling the orientation of the inner frame where the IMU is attached. This firmware allows connectivity via USB, enabling command input through a simulated command line interface.

Concurrently, a Matlab module has been created to acquire data from the calibration platform and the IMU, ensuring proper synchronization for automated calibration.

The calibrating procedure begins with the initialization of the servo-actuators, positioning them at their zero settings. These zero positions, established during installation, align the IMU with the desired initial orientation, ensuring congruence between the body reference system and the inertial reference system:

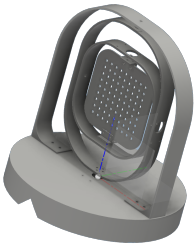

Fig. 1: Calibration platform 3D design

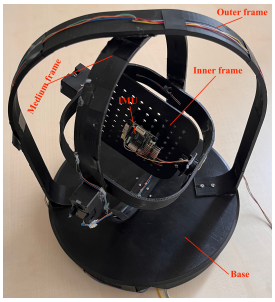

Fig. 2: Installation of the IMU on the calibration platform

$$\phi = 0, \quad \theta = 0, \quad \psi = 0$$

This configuration ensures that the plate on which the Inertial Measurement Unit (IMU) is parallel to the base.

The initial data acquisition phase is needed to calibrate the accelerometer. The IMU is systematically oriented in $N_\Theta \geq 4$ configurations, with angles varying as follows:

$$\begin{array}{rcl} \phi & \in & [-180, 180]\,\text{deg} \\ \theta & \in & [-90, 90]\,\text{deg} \\ \psi & \in & [-180, 180]\,\text{deg} \end{array}$$

This provides a comprehensive coverage of the orientation space.

Subsequently, data acquisition for gyroscope calibration starts. The platform undergoes $N_\omega \geq 2$ rotations of 2 seconds around each axis at varying angular velocities:

$$\begin{array}{rcl} \tilde{y}_x^g & \in & [10, 60]\,\text{deg/s} \\ \tilde{y}_y^g & \in & [10, 60]\,\text{deg/s} \\ \tilde{y}_z^g & \in & [10, 60]\,\text{deg/s} \end{array}$$

This step ensures accurate calibration across a range of rotational speeds.

Finally, the data acquisition for magnetometer calibration takes place. The platform executes a motion designed to cover all possible orientations by describing a sphere at a constant speed r. This is achieved by fixing angles as follows:

$$\phi \in [-180, 180]\,\text{deg}, \quad \theta \in [-90, 90]\,\text{deg}$$

with a step size of $\Delta = 10$ deg.

The adopted rotation sequence allows for satisfying the different characteristics of the three sensors [27]. Indeed, while accelerometers and magnetometers require static or quasi-static measurements (with angular velocities less than 0.6 rad/s), the gyroscope needs to be excited by rotational motions at non-zero angular speed.

IV. Experimental Results

To assess the performance of the proposed calibration platform, experimental tests were conducted. In particular, the proposed calibration platform has been used to collect raw data from an InvenSense MPU-6050 IMU, composed of a 3-axis gyroscope, a 3-axis accelerometer, and a Honeywell HMC5883L 3-axis magnetometer. The full scale parameters are set at $\pm 4\,g$ for the accelerometer, $\pm 500\,\frac{deg}{s}$ for the gyroscope and $\pm 8\,G$ for the magnetometer. Scale factor parameters for the accelerometer, gyroscope, and magnetometer, as indicated in the datasheet, are the following:

$$k_{11}^a = k_{22}^a = k_{33}^a = 1.197 \cdot 10^{-3}\,\frac{m}{s^2}$$

$$k_{11}^g = k_{22}^g = k_{33}^g = 1.527 \cdot 10^{-}2\,\frac{deg}{s}$$

$$k_{11}^m = k_{22}^m = k_{33}^m = 7.299 \cdot 10^{-4}\,G$$

By using the measurements from the uncalibrated sensors in the solution of the problems defined in (2) and (3), it was possible to derive the calibration matrices, presented in (4), (6), and (8), and the bias vectors, presented in (5), (7), and (9).

$$\boldsymbol{K}^a = \begin{bmatrix} -1.78 * 10^{-5} & 1.20 * 10^{-3} & -2.32 * 10^{-6} \\ -6.17 * 10^{-6} & 3.13 * 10^{-6} & 1.20 * 10^{-3} \\ -1.20 * 10^{-3} & -2.12 * 10^{-5} & -1.18 * 10^{-5} \end{bmatrix} \frac{m}{s^2} \quad (4)$$

$$\boldsymbol{b}^a = \begin{bmatrix} 1.90 * 10^{-3} \\ 2.56 * 10^{-1} \\ 1.27 * 10^{-1} \end{bmatrix} \frac{m}{s^2} \quad (5)$$

$$\boldsymbol{K}^g = \begin{bmatrix} 1 * 10^{-4} & -1.42 * 10^{-2} & -5.60 * 10^{-4} \\ 1.9 * 10^{-4} & -1.10 * 10^{-4} & -1.15 * 10^{-2} \\ 1.49 * 10^{-2} & -3.08 * 10^{-5} & 2.80 * 10^{-4} \end{bmatrix} \frac{deg}{s} \quad (6)$$

$$\boldsymbol{b}^g = \begin{bmatrix} 0.1 \\ 0.02 \\ 0.04 \end{bmatrix} \frac{deg}{s} \quad (7)$$

$$\boldsymbol{K}^m = \begin{bmatrix} 6.69 * 10^{-4} & 1.70 * 10^{-3} & 6.07 * 10^{-4} \\ -1.90 * 10^{-3} & 5.74 * 10^{-4} & 1.87 * 10^{-4} \\ 4.21 * 10^{-5} & -5.71 * 10^{-4} & 2 * 10^{-3} \end{bmatrix} G \quad (8)$$

$$\boldsymbol{b}^m = \begin{bmatrix} -2.67 * 10^{-1} \\ -1.24 * 10^{-1} \\ -2.28 * 10^{-1} \end{bmatrix} G \quad (9)$$

We tested the calibration procedure using the Inertial Measurement Unit (IMU) to estimate its attitude. We compared the results with those achievable using only the calibration parameters from the datasheet. The attitude estimation was

implemented by employing an Extended Kalman Filter (EKF) based on the following model:

$$\dot{\boldsymbol{\xi}}(t) = \boldsymbol{f}(\boldsymbol{\xi}(t)) + \boldsymbol{w}(t) \tag{10}$$

where $\boldsymbol{\xi}(t) = \left[\boldsymbol{q}(t)^T, \boldsymbol{\omega}(t)^T\right]^T$ is the state vector, $\boldsymbol{f}(\boldsymbol{\xi}(t))$ is the non-linear state transition function, $\boldsymbol{w}(t) = [\boldsymbol{w}_q(t)^T, \boldsymbol{w}_\omega(t)]$ represents the overall process noise vector. Vectors $\boldsymbol{q}(t) = [q_0(t), q_1(t), q_2(t), q_3(t)]^T$ and $\boldsymbol{\omega}(t) = [\omega_x(t), \omega_y(t), \omega_z(t)]^T$ represent the quaternion [26] and the angular velocity vectors, defined in the body frame, whose dynamics can be expressed as follows:

$$\begin{cases} \dot{\boldsymbol{q}}(t) = \frac{1}{2}\boldsymbol{Q}(\boldsymbol{\omega}(t)) \cdot \boldsymbol{q}(t) + \boldsymbol{w}_q(t) \\ \dot{\boldsymbol{\omega}}(t) = \boldsymbol{w}_\omega(t) \end{cases} \tag{11}$$

where the matrix $\boldsymbol{Q}(\boldsymbol{\omega}(t))$ is

$$\boldsymbol{Q}(\boldsymbol{\omega}(t)) = \begin{bmatrix} 0 & -\omega_x(t) & -\omega_y(t) & -\omega_z(t) \\ \omega_x(t) & 0 & \omega_z(t) & -\omega_y(t) \\ \omega_y(t) & -\omega_z(t) & 0 & \omega_x(t) \\ \omega_z(t) & \omega_y(t) & -\omega_x(t) & 0 \end{bmatrix} \tag{12}$$

Similarly, the output model is defined as follows:

$$\boldsymbol{z}(t) = \boldsymbol{h}(\boldsymbol{\xi}(t)) + \boldsymbol{\nu}(t) \tag{13}$$

where $\boldsymbol{z}(t) = [\boldsymbol{z}^{aT}(t), \boldsymbol{z}^{mT}(t), \boldsymbol{z}^{gT}(t)]^T$ is the output vector at time instant t, $\boldsymbol{h}(\cdot)$ is the observation model, and $\boldsymbol{\nu}(t)$ is the measurement noise. The process noise $\boldsymbol{w}(t)$ and measurement noise $\boldsymbol{\nu}(t)$ are assumed mutually uncorrelated and white Gaussian, with covariance matrices $\boldsymbol{W}(t)$ and $\boldsymbol{R}(t)$, respectively.

The observation model $\boldsymbol{h}(\cdot)$ is defined as follows:

$$\boldsymbol{h}(\boldsymbol{\xi}(t)) = \begin{cases} \boldsymbol{R}_{BE}(\boldsymbol{q}(t)) \cdot [0, 0, g]^T \\ \boldsymbol{R}_{BE}(\boldsymbol{q}(t)) \cdot \mathcal{M}_E \\ \boldsymbol{\omega}(t) \end{cases} \tag{14}$$

with $\boldsymbol{R}_{BE}(\boldsymbol{q}(t))$ representing the rotation matrix from the NED reference frame to the body frame in quaternion form and g being the gravity acceleration.

To highlight the positive effects of the calibration process, the test involves the rotation of the Inertial Measurement Unit (IMU) starting from a horizontal position ($\phi = 0$, $\theta = 0$, and $\psi = 0$), reproducing nine distinct maneuvers around the three axes (X_B, Y_B, Z_B): three roll maneuvers of approximately 15, 30, and -30 deg; three pitch maneuvers of approximately 15, 30, and -30 deg; and finally, three yaw maneuvers of approximately 15, 30, and -30 deg. The test is repeated twice to verify the repeatability of the experiment.

Figures 3a, 3b, and 3c depict the attitude estimation results obtained with the Inertial Measurement Unit (IMU) using the two calibration versions: the dashed green line represents the outcomes achieved with the constructed platform (ϕ_c, θ_c, and ψ_c), while the solid blue line represents the results using the scale factors provided in the datasheet (ϕ_{ds}, θ_{ds}, and ψ_{ds}). The black dashed line represents the reference values (ϕ_{ref}, θ_{ref}, and ψ_{ref}).

It is noteworthy that the absence of well-executed calibration leads to a significant error due to cross-correlation between the axes. Referring to Figure 3, on the tested IMU,

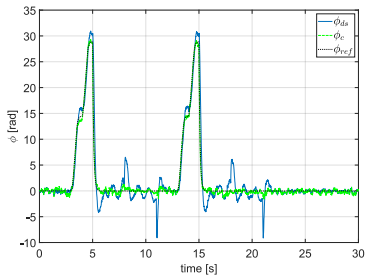

(a)

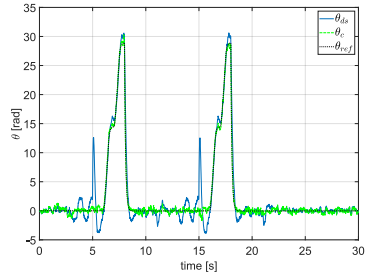

(b)

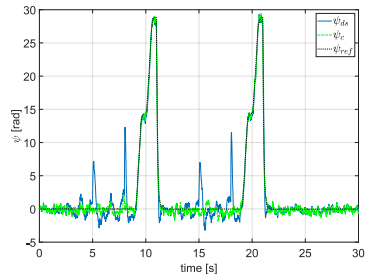

(c)

Fig. 3: Comparison of the estimates of the attitude angles.

the imperfect orthogonality of the sensor axes can result in an error of approximately 7 deg for ϕ_{ds} during a pitch maneuver of 30 deg and approximately 9 deg during a yaw maneuver of 30 deg. In the same way, similar cross-correlations exist during roll and yaw maneuvers.

V. CONCLUSIONS

The presented low-cost and portable IMU calibration platform, featuring three servomotors enabling rotations around orthogonal axes, proves to be an effective solution for mitigating errors inherent in low-cost IMUs. The platform facilitates both static and dynamic calibration, providing the necessary parameters to enhance the accuracy of attitude estimation.

The performance evaluation highlights the substantial difference in attitude estimation between an IMU calibrated with and without the use of the proposed platform. This underscores the efficacy of the platform in significantly improving the precision and reliability of low-cost IMUs, further emphasizing its relevance in enhancing the overall performance of small UAVs equipped with MEMS-based IMUs.

ACKNOWLEDGMENT

The authors wish to thank students Valeria Pennino, Sofia Serio, and Fabio Vaccaro for their invaluable support to build the calibration platform and during the laboratory tests.

REFERENCES

[1] Batu Candan and Halil Ersin Soken. "Robust attitude estimation using IMU-only measurements". In: *IEEE Transactions on Instrumentation and Measurement* 70 (2021), pp. 1–9.

[2] Paul D Groves. "Navigation using inertial sensors [Tutorial]". In: *IEEE Aerospace and Electronic Systems Magazine* 30.2 (2015), pp. 42–69.

[3] David Tedaldi, Alberto Pretto, and Emanuele Menegatti. "A robust and easy to implement method for IMU calibration without external equipments". In: *2014 IEEE International Conference on Robotics and Automation (ICRA)*. IEEE. 2014, pp. 3042–3049.

[4] Oliver J Woodman. *An introduction to inertial navigation*. Tech. rep. University of Cambridge, Computer Laboratory, 2007.

[5] Maryam Kiani, Seid H Pourtakdoust, and Ali Akbar Sheikhy. "Consistent calibration of magnetometers for nonlinear attitude determination". In: *measurement* 73 (2015), pp. 180–190.

[6] "IEEE Standard for Inertial Systems Terminology". In: *IEEE Std. 1559-2009 (Revision of IEEE Std 1559-2009)* (November 2022), pp. 1–46.

[7] Kseniya I Goryanina and Alexandr D Lukyanov. "Recursive least squares method for identification of MEMS orientation sensors parameters". In: *2019 International Conference on Industrial Engineering, Applications and Manufacturing (ICIEAM)*. IEEE. 2019, pp. 1–6.

[8] Egidio D'Amato et al. "UKF-based fault detection and isolation algorithm for IMU sensors of Unmanned Underwater Vehicles". In: *2021 International Workshop on Metrology for the Sea; Learning to Measure Sea Health Parameters (MetroSea)*. IEEE. 2021, pp. 371–376.

[9] Egidio D'Amato et al. "Fault tolerant low cost IMUS for UAVs". In: *2017 IEEE International Workshop on Measurement and Networking (M&N)*. IEEE. 2017, pp. 1–6.

[10] Egidio D'Amato et al. "UAV sensor FDI in duplex attitude estimation architectures using a set-based approach". In: *IEEE Transactions on Instrumentation and Measurement* 67.10 (2018), pp. 2465–2475.

[11] Egidio D'Amato et al. "A particle filtering approach for fault detection and isolation of UAV IMU sensors: Design, implementation and sensitivity analysis". In: *Sensors* 21.9 (2021), p. 3066.

[12] Alessia Ferraro and Valerio Scordamaglia. "A set-based approach for detecting faults of a remotely controlled robotic vehicle during a trajectory tracking maneuver". In: *Control Engineering Practice* 139 (2023), p. 105655.

[13] Wanliang Zhao et al. "Navigation grade MEMS IMU for a satellite". In: *Micromachines* 12.2 (2021), p. 151.

[14] S Zotov et al. "Quartz MEMS Accelerometer for EMCORE Inertial Technology from Tactical to High-End Navigation". In: *2022 DGON Inertial Sensors and Systems (ISS)*. IEEE. 2022, pp. 1–20.

[15] Gökçen Aslan Aydemir and Afşar Saranlı. "Characterization and calibration of MEMS inertial sensors for state and parameter estimation applications". In: *Measurement* 45.5 (2012), pp. 1210–1225.

[16] Ping Zhang, Xin Liu, and Guanglong Du. "Online robot auto-calibration using IMU with CMAC and EKF". In: *2015 IEEE International Conference on Cyber Technology in Automation, Control, and Intelligent Systems (CYBER)*. IEEE. 2015, pp. 896–901.

[17] Giorgio de Alteriis et al. "Use of consumer-grade MEMS inertial sensors for accurate attitude determination of drones". In: *2020 IEEE 7th International Workshop on Metrology for AeroSpace (MetroAeroSpace)*. IEEE. 2020, pp. 534–538.

[18] Umar Qureshi and Farid Golnaraghi. "An algorithm for the in-field calibration of a MEMS IMU". In: *IEEE Sensors Journal* 17.22 (2017), pp. 7479–7486.

[19] Jixin Lv et al. "A method of low-cost IMU calibration and alignment". In: *2016 IEEE/SICE International Symposium on System Integration (SII)*. IEEE. 2016, pp. 373–378.

[20] Ying-Chih Lai, Shau-Shiun Jan, and Fei-Bin Hsiao. "Development of a low-cost attitude and heading reference system using a three-axis rotating platform". In: *Sensors* 10.4 (2010), pp. 2472–2491.

[21] Chao-Chung Peng, Jing-Jie Huang, and Ho-Yang Lee. "Design of an embedded icosahedron mechatronics for robust iterative IMU calibration". In: *IEEE/ASME Transactions on Mechatronics* 27.3 (2021), pp. 1467–1477.

[22] David Titterton and John L Weston. *Strapdown inertial navigation technology*. Vol. 17. IET, 2004.

[23] Valérie Renaudin, Muhammad Haris Afzal, Gérard Lachapelle, et al. "Complete triaxis magnetometer calibration in the magnetic domain". In: *Journal of sensors* 2010 (2010).

[24] Bin Fang, Wusheng Chou, and Li Ding. "An optimal calibration method for a MEMS inertial measurement unit". In: *International Journal of Advanced Robotic Systems* 11.2 (2014), p. 14.

[25] Rui Zhang, Fabian Hoflinger, and Leonhard M Reind. "Calibration of an IMU using 3-D rotation platform". In: *IEEE sensors Journal* 14.6 (2014), pp. 1778–1787.

[26] Roberto G Valenti, Ivan Dryanovski, and Jizhong Xiao. "Keeping a good attitude: A quaternion-based orientation filter for IMUs and MARGs". In: *Sensors* 15.8 (2015), pp. 19302–19330.

[27] Chi Ming Cheuk et al. "Automatic calibration for inertial measurement unit". In: *2012 12th International Conference on Control Automation Robotics & Vision (ICARCV)*. IEEE. 2012, pp. 1341–1346.